人間発達科学部紀要　第２巻第１号：13－36（２００７）

# Numerical Simulation of Immiscible Two-fluid Flows by Flux-free Finite Element Method

Katsushi Ohmori and Hiroshi Okumura

**Abstract**

The purpose of this paper is to present a numerical model for immiscible incompressible two-fluid flows, which preserves the discrete mass of the fluid more highly. This method is derived from the variational formulation including the flux-free constraint for the Navier-Stokes equations by the Lagrange multiplier technique and is implemented by the fractional projection finite element scheme. The interface is expressed by the level set of the pseudo-density function, so that we also solve the transport equation by the finite element method. Finally we give some numerical results to validate our proposed method.

Keywords : flux-free, finite element method, Lagrange multiplier, immiscible two-fluid flows, mass preserving

## 1 Introduction

In numerical simulations for the free interface flow problems, it is needless to say that it is important to reproduce the interface precisely, however, there is also another important issue concerning the *mass preserving*. In fact, although in the immiscible incompressible two-fluid flows the mass of the fluid should be preserved in all time due to the incompressibility and immiscibility, we have often experienced the *gain* or *loss* of the mass of both fluids in the numerical simulation of such problems [9]. Therefore in this paper we are concerned with the new finite element method for immiscible incompressible two-fluid flows which ensures the good mass preserving. One of the cause of such phenomena is that the numerical flux of the velocity of each fluid through the interface does not equal zero. So that, introducing the flux functional on the interface, we propose the flux-free finite element method in the *Eulerlian* framework, which is derived from the variational formulation including the flux-free constraint for the Navier-Stokes equations by the Lagrange multiplier technique. For the mathematical foundation for this method we refer to Ohmori and Saito [11], where the well-posedness of the stationary Stokes problem under the discrete inf-sup condition and the basic error estimates have been shown. Similar idear using the Lagrange multiplier technique with flux functional have already proposed by Formaggia et al. [4] to ensure the mass preserving of the fluid for the free

interface problems as an application of the numerical method for the blood flow problems in the cardiovascular system. However, their method is essentially based on the *Lagrangian* approach. In the method of this type, since the location of the interface is explicitly tracked using meshes moving with the interface, it needs a costly resoning mesh procedure when the mesh become distorted. On the contrary, in Eulerian approach the interface is captured on a simple fixed mesh by the pseudo-density function or level set function. Then large deformations and topological changes can also be handled easily. Therefore it is meaningful to consider the mass preserving finite element method in the *Eulerian* framework.

This paper is organized as follows. In Sect.2 we present a model problem for immiscible incompressible two-fluid flows. In Sect.3 we consider the flux-free finite element method and show the numerical algorithm of our method. In Sect.4 we show the approximation of the flux-functional. Finally, Sect.5 shows the numrical results illustrating the effectiveness of our proposed method.

# 2 Mathematical model

Let $\Omega$ be a bounded domain of $R^2$ with the boundary $\Gamma$. The domain $\Omega$ consisits of two time-dependent subdomains $\Omega_\alpha = \Omega_\alpha(t), \alpha = 1, 2$, such that

$$\overline{\Omega} = \overline{\Omega_1(t)} \cup \overline{\Omega_2(t)} \quad \text{and} \quad \Omega_1(t) \cap \Omega_2(t) = \emptyset \quad \text{for} \quad 0 \le t < T, \tag{2.1}$$

where $T$ is a constant. Subdomain $\Omega_\alpha$ is filled with the $fluid\#\alpha$ with density $\rho_\alpha$ and viscosity $\mu_\alpha$. We assume that two fluids are both viscous, incompressible and immiscible. Furthermore, we assume that the physical effects of the surface tension on the interface are negligible for simplicity. For any $0 \le t < T$ let $\Sigma$ be the interface between the two fluids :

$$\Sigma = \Sigma(t) = \overline{\Omega_1(t)} \cap \overline{\Omega_2(t)}. \tag{2.2}$$

Here we set $\Gamma_\alpha = \partial\Omega_\alpha \backslash \Sigma$. Let $\mathbf{n}^{(\alpha)}$ and $\boldsymbol{\tau}^{(\alpha)}$ be the outward unit normal vector and the unit tangential vector to the boundary $\partial\Omega_\alpha$, respectively. It is clear that $\mathbf{n}^{(2)} = -\mathbf{n}^{(1)}$ on the interface $\Sigma$. The governing equations for immiscible incompressible two-fluid flows can be written by the Navier-Stokes equations :

$$\begin{cases} \rho_\alpha \left( \dfrac{\partial \mathbf{u}^{(\alpha)}}{\partial t} + (\mathbf{u}^{(\alpha)} \cdot \nabla)\mathbf{u}^{(\alpha)} \right) = \nabla \cdot \boldsymbol{\sigma}^{(\alpha)} + \rho_\alpha \mathbf{F}^{(\alpha)} & \text{in } \Omega_\alpha, \\ \operatorname{div} \mathbf{u}^{(\alpha)} = 0 & \text{in } \Omega_\alpha, \\ \mathbf{u}^{(\alpha)} \cdot \mathbf{n}^{(\alpha)} = 0 & \text{on } \Gamma_\alpha, \\ (\boldsymbol{\sigma}^{(\alpha)}\, \mathbf{n}^{(\alpha)}) \cdot \boldsymbol{\tau}^{(\alpha)} = 0 & \text{on } \Gamma_\alpha, \\ \mathbf{u}^{(\alpha)}|_{t=0} = \mathbf{u}_0^{(\alpha)} & \text{in } \Omega_\alpha, \end{cases} \tag{2.3}$$

where $\mathbf{u}^{(\alpha)}$ is the velocity vector, $p^{(\alpha)}$ is the pressure, $\mathbf{F}^{(\alpha)}$ is the body force per unit volume and $\mathbf{u}_0^{(\alpha)}$ is the prescribed divergence-free velocity. The stress

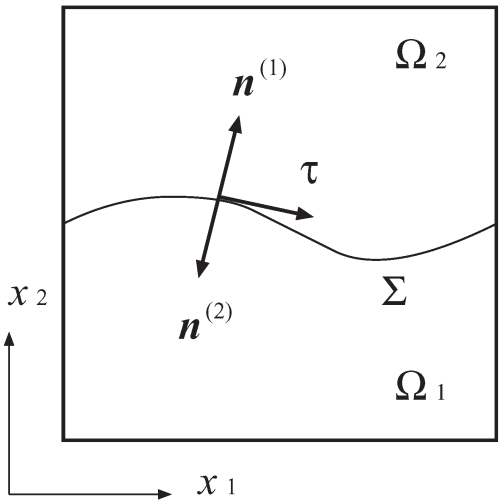


Figure 1: Two-fluid flow problem

tensor $\boldsymbol{\sigma}^{(\alpha)}$ is defined as

$$\boldsymbol{\sigma}^{(\alpha)} = -p^{(\alpha)}\mathbf{I} + 2\mu_\alpha\, D(\mathbf{u}^{(\alpha)}), \tag{2.4}$$

where $\mathbf{I}$ is the identity tensor and $D(\mathbf{u}^{(\alpha)})$ is the deformation tensor :

$$D(\mathbf{u}^{(\alpha)}) = \frac{1}{2}(\nabla\mathbf{u}^{(\alpha)} + (\nabla\mathbf{u}^{(\alpha)})^T) \tag{2.5}$$

Furthermore we assume the following transmission condition on the interface :

$$\begin{cases} \mathbf{u}^{(1)} = \mathbf{u}^{(2)} & \text{on } \Sigma, \\ \boldsymbol{\sigma}^{(1)}\cdot\mathbf{n}^{(1)} - \boldsymbol{\sigma}^{(2)}\cdot\mathbf{n}^{(1)} = \sigma\kappa\mathbf{n}^{(1)} & \text{on } \Sigma, \end{cases} \tag{2.6}$$

where $\sigma$ is the surface tension coefficient and $\kappa$ is the curvature of the interface $\Sigma$. Condition (2.6) shows the continuity of the velocity and of the normal component of the stress tensor at the interface, respectively. For simplicity we assume that the surface tension effects are negligible, that is $\sigma = 0$.

In order to describe the evolution of the interface we assume that the interface $\Sigma = \Sigma(t)$ is defined by the level set of the pseudo-density function $\varphi = \varphi(\mathbf{x}, t)$ as follows

$$\Sigma = \{\mathbf{x} = (x_1, x_2)\,|\,\varphi(\mathbf{x}, t) = 1/2\},\ \text{for } 0 \le t < T. \tag{2.7}$$

Since a particle on the interface remains on the interface for any time $t \in [0, T)$ by the immiscibility, the pseudo-density function $\varphi$ satisfies the following transport equation :

$$\begin{cases} \dfrac{\partial\varphi}{\partial t} + \mathbf{u}\cdot\nabla\varphi = 0 & \text{in } \Omega\times(0,\,T), \\ \varphi|_{t=0} = \varphi_0 & \text{in } \Omega, \end{cases} \tag{2.8}$$

where $\mathbf{u}|_{\Omega_\alpha} = \mathbf{u}^{(\alpha)}$. As for the initial condition $\varphi_0$ we shall take the smooth function such that

$$\varphi_0 = \begin{cases} 1 & \text{in } \Omega_1, \\ 1/2 & \text{on } \Sigma, \\ 0 & \text{in } \Omega_2, \end{cases} \tag{2.9}$$

Furthermore the unit normal vector on the interface $\Sigma$ can be expressed by the pseudo-density function $\varphi$ as follows :

$$\mathbf{n}^{(1)} = \frac{\nabla\varphi}{|\nabla\varphi|}\Big|_{\varphi=1/2}. \tag{2.10}$$

Thus we find that immiscible incompressible two-fluid flows are the problem coupling the Navier-Stokes equations (2.3) and the transport equation (2.8).

On the other hand, it is clear that the flux of the velocity of each fluid through the interface $\Sigma$ equals 0 in immiscible two-fluid flows by the incompressibility condition and the free-slip boundary condition, (*i.e.*)

$$\int_\Sigma \mathbf{u}^{(\alpha)} \cdot \mathbf{n}^{(\alpha)} d\gamma = 0. \tag{2.11}$$

Since it holds that for $0 < t_1 < t_2 < T$

$$\rho_\alpha \,\mathrm{meas}(\Omega_\alpha(t_2)) - \rho_\alpha \,\mathrm{meas}(\Omega_\alpha(t_1)) = \int_{t_1}^{t_2} \rho_\alpha \int_\Sigma \mathbf{u}^{(\alpha)} \cdot \mathbf{n}^{(\alpha)} \,\mathrm{d}\gamma \,\mathrm{d}t, \tag{2.12}$$

the mass of each fluid should be preserved on any time $t \in [0, T)$ by (2.11), however, in many numerical simulations of these problems we have often experienced the *gain or loss* of the mass of the fluid. This is caused by the fact that the discrete flux of the velocity on the interface $\Sigma$ does not vanish.

Therefore, introducing the flux functional $\langle \phi,\, \mathbf{u}^{(\alpha)} \rangle_\Sigma$ by

$$\langle \phi,\, \mathbf{u}^{(\alpha)} \rangle_\Sigma = \int_\Sigma \mathbf{u}^{(\alpha)} \cdot \mathbf{n}^{(\alpha)} \,\mathrm{d}\gamma, \tag{2.13}$$

we propose the flux-free finite element method which is derived from the variational formulation including the flux-free constraint for the Navier-Stokes equations by the Lagrange multiplier technique.

# 3 Flux-free finite element method

## 3.1 Variational formulation

In this section, we consider the flux-free finite element method for the Navier-Stokes equations (2.3). Let $\{\mathcal{T}_h\}$ be a family of triangulations for the domain $\overline{\Omega}$ such that

$$\overline{\Omega} = \cup_{K \in \mathcal{T}_h} K. \tag{3.1}$$

Let $\mathbf{X} = H^1(\Omega)^2$ and $Q = L^2_0(\Omega)$ be two real Hilbert space with the norms $\|\cdot\|_X$ and $\|\cdot\|_Q$, respectively, Furthermore, let $\mathbf{X}_h$ and $Q_h$ be the conforming finite element spaces such that a usual *inf-sup* condition. Here we set

$$\mathbf{X}_h^0 = \{\mathbf{v}_h \in \mathbf{X}_h \mid \mathbf{v}_h \cdot \mathbf{n}_h = 0 \text{ on } \Gamma\}, \tag{3.2}$$

where $\mathbf{n}_h$ is the approximation of $\mathbf{n}^{(1)}$.

Then we consider the following semi-discrete finite element approximation :

Find $(\mathbf{u}_h,\, p_h,\, \lambda_h) \in \mathbf{X}_h^0 \times Q_h \times \mathbf{R}$ such that for $0 < t < T$

$$(\Pi_h^\lambda) \begin{cases} (\rho(\dfrac{\partial \mathbf{u}_h}{\partial t} + \mathbf{u}_h \cdot \nabla \mathbf{u}_h),\, \mathbf{v}_h) + 2(\mu\, D(\mathbf{u}_h),\, D(\mathbf{v_h})) & \\ -(p_h,\, \operatorname{div} \mathbf{v}_h) + \lambda_h \langle \phi,\, \mathbf{v}_h \rangle_\Sigma = (\rho \mathbf{F},\, \mathbf{v}_h) & \forall \mathbf{v}_h \in \mathbf{X}_h^0, \\ (q_h,\, \operatorname{div} \mathbf{u}_h) = 0 & \forall q_h \in Q_h, \\ \xi_h \langle \phi,\, \mathbf{u}_h \rangle_\Sigma = 0 & \forall \xi_h \in \mathbf{R}, \end{cases} \tag{3.3}$$

On the other hand, we also consider the finite element approximation for the transport equation (2.8):

Find $\varphi_h \in X_h$ such that for $0 < t < T$

$$\begin{cases} (\dfrac{\partial \varphi_h}{\partial t},\, \theta_h) + (\mathbf{u}_h \cdot \nabla \varphi_h,\, \theta_h) = 0 \quad \forall \theta_h \in X_h, \\ \varphi_h|_{t=0} = \varphi_{0h}, \end{cases} \tag{3.4}$$

where $\varphi_{0h}$ is some approximation of $\varphi_0$.

In order to resolve such a nonlinear interaction we first resolve the Navier-Stokes equations (3.3) with a fixed known interface, then, using computed velocity fields, we resolve the transport equation (3.4). Having found the new interface position we can calculate its normal vector, and, thus the density and viscosity to be used on the next time step in the Navier-Stokes equations. For more detail of the computational algorithm we discuss in the following subsection.

## 3.2 Flux-free finite element approximation

For the finite element approximration for the Navier-Stokes equations and the transport equation we use the MINI element ($P_1 \oplus Bubble/P_1$) and $P_1 \oplus Bubble$, respectively.

First, we define the finite element spaces using the MINI element as follows :

$$\begin{cases} X_h = \{v_h \in C(\overline{\Omega}) \mid \mathbf{v}_h|_K \in P^1(K) \ \ \forall K \in \mathcal{T}_h\} \bigoplus_{K \in \mathcal{T}_h} B(K), \\ Q_h = \{q_h \in C(\overline{\Omega}) \mid q_h|_K \in P^1(K) \ \ \forall K \in \mathcal{T}_h,\ \displaystyle\int_\Omega q_h \,\mathrm{d}x = 0\}, \end{cases} \tag{3.5}$$

where $P^1(K)$ is a set of linear polynomials on $K \in \mathcal{T}_h$ and $B(K)$ is spanned by a bubble function $b(K) = \lambda_1\lambda_2\lambda_3 \in H_0^1(K)$. In practical computation we use the bubble function with a *scaling parameter* [13]. Here we set $\mathbf{X}_h = X_h \times X_h$.

In order to define a full discretization of $(\Pi_h)$, we consider the uniform mesh for the time variable $t$ and define

$$t_n = n\,\Delta t \quad \text{for } n = 0,\, 1,\, 2,\, \cdots,\, [T/\Delta t], \tag{3.6}$$

where $\Delta t > 0$ is a time-step. We introduce the following bilinear form $a(\cdot,\, \cdot)$ on $\mathbf{X_h} \times \mathbf{X}_h$ :

$$a(\mathbf{u}_h,\, \mathbf{v}_h) = 2(\mu\, D(\mathbf{u}_h),\, D(\mathbf{v}_h)). \tag{3.7}$$

Furthermore, we define a tri-linear form $c(\,\cdot\,;\,\cdot,\,\cdot)$ on $\mathbf{X_h} \times \mathbf{X}_h \times \mathbf{X}_h$ as follows :

$$c(\mathbf{w}_h;\, \mathbf{u}_h,\, \mathbf{v}_h) = \frac{1}{2}\{(\rho(\mathbf{w}_h \cdot \nabla \mathbf{u}_h),\, \mathbf{v}_h) - (\rho(\mathbf{w}_h \cdot \nabla \mathbf{v}_h),\, \mathbf{u}_h)\}. \tag{3.8}$$

Then we consider the following fractional-step projection finite element scheme [10, 12] :

$$\begin{cases} (\rho\dfrac{\mathbf{u}_h^{n+1/2} - \mathbf{u}_h^n}{\Delta t},\, \mathbf{v}_h) + c(\mathbf{u}_h^n;\, \mathbf{u}_h^{n+1/2},\, \mathbf{v}_h) & \\ \qquad\qquad +a(\mathbf{u}_h^{n+1/2},\, \mathbf{v}_h) = (\rho\,\mathbf{F},\, \mathbf{v}_h) & \forall \mathbf{v}_h \in \mathbf{X}_h^0, \\ \mathbf{u}_h^{n+1/2} = \mathbf{0} & \text{on } \Gamma, \end{cases} \tag{3.9}$$

$$\begin{cases} (\rho\dfrac{\mathbf{u}_h^{n+1} - \mathbf{u}_h^{n+1/2}}{\Delta t},\, \mathbf{v}_h) - (p_h^{n+1},\, \operatorname{div} \mathbf{v}_h) & \\ \qquad\qquad +\lambda_h^{n+1}\,\langle \phi,\, \mathbf{v}_h\rangle_\Sigma = 0 & \forall \mathbf{v}_h \in \mathbf{X}_h^0, \\ (q_h, \operatorname{div} \mathbf{u}_h^{n+1}) = 0 & \forall q_h \in Q_h, \\ \xi_h\,\langle \phi,\, \mathbf{u}_h^{n+1}\rangle_\Sigma = 0 & \forall \xi_h \in \mathbf{R}. \end{cases} \tag{3.10}$$

This projection method consists of the viscous step (3.9) and the projection step (3.10). Equation (3.9) shows that the intermediate velocity $\mathbf{u}_h^{n+1/2}$ is computed as the solution of a discretized momentum equation without the pressure term. Ignoring the flux functional term, equation (3.10) shows that the intermediate velocity $\mathbf{u}_h^{n+1/2}$ is decomposed into the sum of a solenoidal velocity $\mathbf{u}_h^{n+1}$ and the gradient of a scaler function propotional to the pressure $p_h^{n+1}$.

On the other hand, we have to solve the transport equation in order to determine the density $\rho$ and viscosity $\mu$. In this paper we consider the following *pure* advection problem with fixed velocity in each time interval $(t_n,\, t_{n+1}]$ :

$$\begin{cases} (\dfrac{\varphi_h^{n+1} - \varphi_h^n}{\Delta t},\, \theta_h) + (\mathbf{u}_h^* \cdot \nabla \varphi_h^{n+1},\, \theta_h) = 0 & \forall \theta_h \in X_h. \\ \varphi_h^0 \text{ is given,} \end{cases} \tag{3.11}$$

where $\mathbf{u}_h^*$ is a given constant vector and $\varphi_h^0$ is an approximation of $\varphi_0$ shown in Figure 2. In practice, for example, we take $\mathbf{u}_h^* = \mathbf{u}_h^{n+1}$.

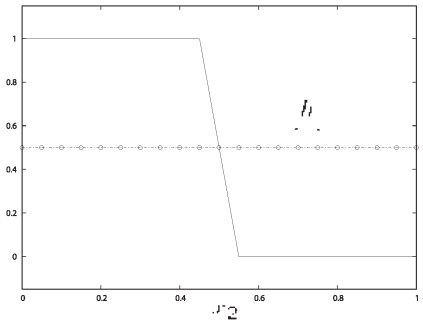


Figure 2: Initial value $\varphi_h^0$

The values of $\rho$ and $\mu$ in equations (3.9)-(3.10) are approximated by the piecewise constant on $K \in \mathcal{T}_h$, respectively :

$$\begin{cases} \rho|_K = \overline{\varphi}_K^n \, \rho_1 + (1 - \overline{\varphi}_K^n) \, \rho_2, \\ \mu|_K = \overline{\varphi}_K^n \, \mu_1 + (1 - \overline{\varphi}_K^n) \, \mu_2, \end{cases} \tag{3.12}$$

where $\overline{\varphi}_K^n = \frac{1}{3}\{H_c(\varphi_{1,K}^n) + H_c(\varphi_{2,K}^n) + H_c(\varphi_{3,K}^n)\}$, $\varphi_{i,K}^n, 1 \leq i \leq 3$, is the approximation of $\varphi_h^n$ at the vertex $K_i$ of $K \in \mathcal{T}_h$ and $H_c(\cdot)$ is a *cut-off* function defined by

$$H_c(\varphi) = \begin{cases} 1 & (\varphi \geq 1), \\ \varphi & (0 < \varphi < 1), \\ 0 & (\varphi \leq 0). \end{cases} \tag{3.13}$$

# 4 Approximation of flux functional

As for the approximation of the flux functional, it is necesarry to clarify the definitions of the approximate interface $\Sigma_h$ and the approximation of the normal vector $\mathbf{n}$, respectively. From the definition of the interface $\Sigma$ it is natural to define the approximate interface $\Sigma_h$ by the 1/2-level set of $\varphi_h^n$. Since $\varphi_h^n$ is approximated by $P_1 \oplus Bubble$-element, we may assume that the approximate interface $\Sigma_h$ is piecewise linear on $K \in \mathcal{T}_h$. If we approximate $\mathbf{n}$ using (2.10) as follows;

$$\mathbf{n}_h = \frac{\nabla \varphi_h^n}{|\nabla \varphi_h^n|} \quad \text{on } \Sigma_h, \tag{4.1}$$

then $\mathbf{n}_h$ is a constant vector on $K \in \mathcal{T}_h$. So that, we extend $\mathbf{n}_h|_K$ into $\mathbf{n}_h^*|_K \in P_1(K)$ for $K \in \mathcal{T}_h$ by considering the following auxiliary variational problem :

Find $\mathbf{n}_h^* \in \mathbf{W}_h$ such that

$$(\mathbf{n}_h^*,\, \mathbf{w}_h) = (\tilde{\mathbf{n}},\, \mathbf{w}_h) \quad \forall \mathbf{w}_h \in \mathbf{W}_h, \tag{4.2}$$

where

$$\mathbf{W}_h = \left\{ \mathbf{w}_h \in (C(\overline{\Omega}))^2 \mid \mathbf{w}_h \in (P^1(K))^2 \ \ \forall K \in \mathcal{T}_h \right\}, \tag{4.3}$$

and

$$\tilde{\mathbf{n}} = \begin{cases} \mathbf{n}_h|_K & (\Sigma_h \cap K \neq \emptyset \ \ \forall K \in \mathcal{T}_h), \\ \mathbf{0} & (\textit{otherwise}). \end{cases} \tag{4.4}$$

Thus we define the approximate flux functional as follows:

$$\langle \phi,\, \mathbf{u}_h \rangle_{\Sigma_h} = \int_{\Sigma_h} \mathbf{u}_h \cdot \mathbf{n}_h^* \, \mathrm{d}\gamma \quad \forall \mathbf{u}_h \in \mathbf{X}_h. \tag{4.5}$$

Evaluating the line integral by the trapezoidal method, we have the following :

$$\begin{aligned} \langle \phi,\, \mathbf{u}_h \rangle_{\Sigma_h} &= \sum_{K \in \mathcal{T}_h} \int_{\Sigma_h \cap K} \mathbf{u}_h \cdot \mathbf{n}_h^* \, \mathrm{d}\gamma \\ &\approx \sum_{K \in \mathcal{T}_h} \frac{\|\mathbf{x}_a \vec{\mathbf{x}}_b\|_E}{2} (\mathbf{u}_h|_K(\mathbf{x}_a) \cdot \mathbf{n}_h^*|_K(\mathbf{x}_a) + \mathbf{u}_h|_K(\mathbf{x}_b) \cdot \mathbf{n}_h^*|_K(\mathbf{x}_b)), \end{aligned}$$

where $\mathbf{x}_a,\, \mathbf{x}_b \in \partial K \cap \Sigma_h$ and $\| \cdot \|_E$ denotes the Euclidean norm.

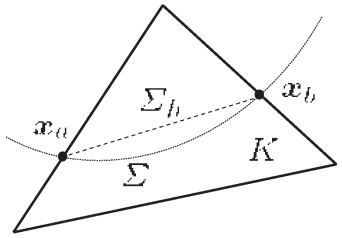


Figure 3: An approximate interface $\Sigma_h$

**Remark 4.1** *Since in the flux-free finite element method we have to evaluate the flux functional* $\langle \phi,\, \mathbf{u}_h \rangle_{\Sigma_h}$ *on all elements* $K \in \mathcal{T}_h$ *and then be assembled into the whole finite element matrix even if the interface* $\Sigma$ *is located anywhere in the domain* $\Omega$ *and has any large deformation and topological change.*

# 5 Numerical experiments

In this section, we give some numerical results to validate our proposed method. The first example is an immiscible two-fluid interface problem [3] and the second one is a sloshing problem [3] in a closed container filled with an immiscible two-fluid which is subjected to a horizontal periodic vibration and the gravity acceleration.

## 5.1 Two-fluid interface problem

We consider a simple two-fluid flows where two immiscible fluids are initially at rest in a closed container $\Omega = (0,1) \times (0,1)$ and the initial interface is stepped with the elevation $\Delta\eta$ from an average height $\eta$. The definition of the problem is illustrated in Figure 4. Fluid properties are shown in Table 1. The computaions were performed on the triangulations based on $20 \times 20$ and $40 \times 40$ regular meshes of the union-jack type. We impose the free-slip condition on the domain boundary. Parameters and conditions are summarized in table 5.1.

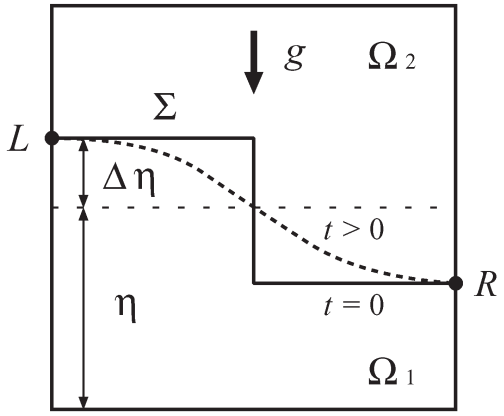


Figure 4: Two–fluid interface problem with initial stepped interface

Table 1: Fluid properties

| set | $\rho_1$ | $\mu_1$ | $\rho_2$ | $\mu_2$ | $\Delta\eta : \eta$ |
|---|---|---|---|---|---|
| A | 1.0 | 0.005 | 0.9 | 0.005 | 2 : 5 |
| B | 4.0 | 0.01 | 1.0 | 0.01 | 1 : 5 |

Table 2: Cases computed for two-fluid interface problem

| case | Mesh (Union-Jack) | Total time $T$ | Time steps $[T/\Delta t]$ | Flux functional | Property set |
|---|---|---|---|---|---|
| A1 | $20 \times 20$ | 100 | 2500 | Yes | A |
| A2 | $20 \times 20$ | 100 | 2500 | No | A |
| A3 | $40 \times 40$ | 100 | 5000 | Yes | A |
| A4 | $40 \times 40$ | 100 | 5000 | No | A |
| B1 | $40 \times 40$ | 80 | 8000 | Yes | B |
| B2 | $40 \times 40$ | 80 | 8000 | No | B |
| B3 | $40 \times 40$ | 80 | 16000 | Yes | B |
| B4 | $40 \times 40$ | 80 | 16000 | No | B |

Figure 5 shows the time histories of elevation of the interface at the left and right sides of container, denoted respectively as L and R, where "with flux functional" denotes the results obtained by our proposed method and "w/o flux functional" denotes the results obtained by the method without the flux functional. From this result we observe that our method gives almost same phenomena as the method without flux functional at least in the behavior at the left and right sides, however, we find that there is a crucial difference between two method from Figure 6. In fact, from this result we can observe that our method gives almost zero flux, while the method without flux functional gives *negative* flux in almost computation time. That is, there is a strong possibility that in the method without flux functional the mass of the $fluid\#1$ increase during the computation time by the sign of the flux. The similar phenomena can be seen in the case of the $40 \times 40$ mesh shown in Figure 7. Such phenomena are remarkable in the case of relative high density ratio (the set B). From Figure 8, we find also the *negative* flux during almost computation time. This also implies the possibility of the mass increasing of $fluid\#1$. In fact from Figure 9 we can observe that the elevation of the interface at right side R keeps up about 2% from the average height since $t = 40$. This means exactly that the mass of the $fluid\#1$ increase. Figure 10 shows the time histories of the Lagrange multiplier for the set A using $20 \times 20$ and $40 \times 40$ meshes, respectively. We find that the absolute value of the Lagrange multiplier is about $10^{-6}$ - $10^{-7}$, and it seems that $|\lambda_h|$ converges to 0 very slowly. Figure 11 shows the velocity vector and the interface and Figure 12 shows iso-contours of the pressure obtained by the proposed method.

## 5.2 Sloshing problem

Sloshing problem consists of looking at the oscillations of the interface between two immiscible fluids in a two-dimensional container $\Omega = (0, 1) \times (0, 1)$ as shown Figure 13. The initial interface is at rest with a flat interface with an average height 0.5. The system is subjected to gravity $g = 9.8$ and a horizontal periodic acceleration with amplitude $A = ag$ and frequency $\omega = 2\pi\beta$. In this example we plan to evaluate the performance of the proposed method for *low* and *high*

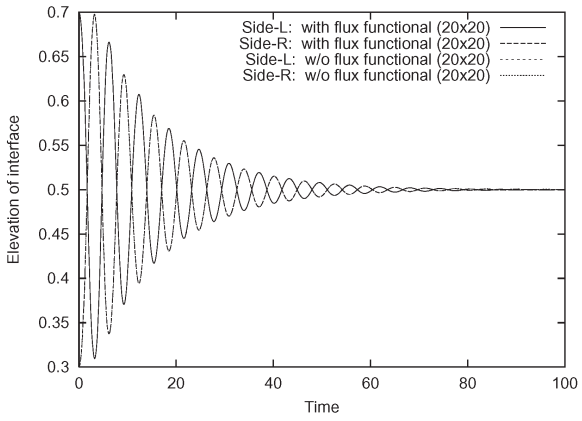


Figure 5: Time history of elevation of the interface at the sides L and R(Case A1 and A2).

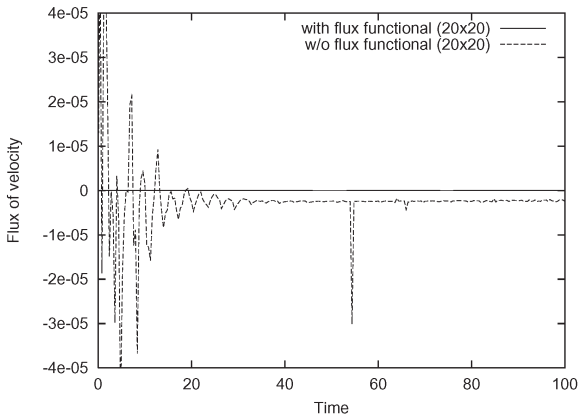


Figure 6: Time history of flux of velocity through the interface.(Case A1 and A2)

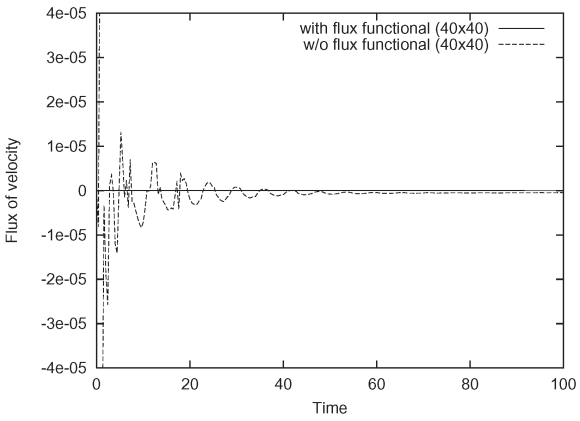


Figure 7: Time history of flux of velocity through the interface(Case A3 and A4).

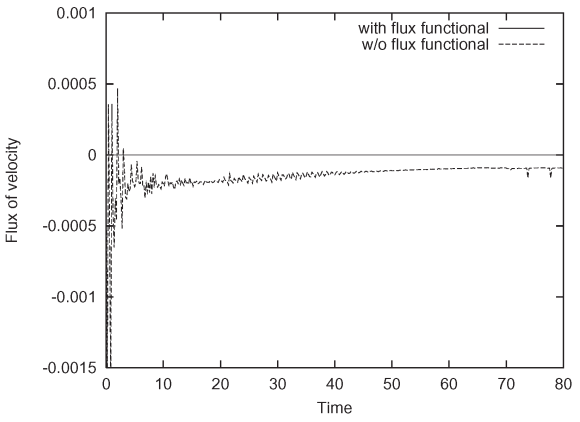


Figure 8: Time history of flux of velocity through the interface(Case B1 and B2).

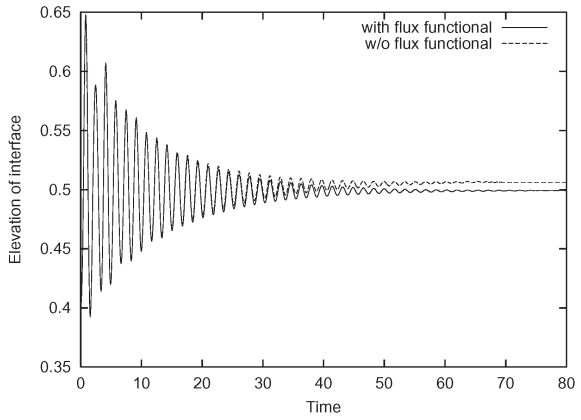


Figure 9: Time history of elevation of the interface at the side R(Case B1 and B2).

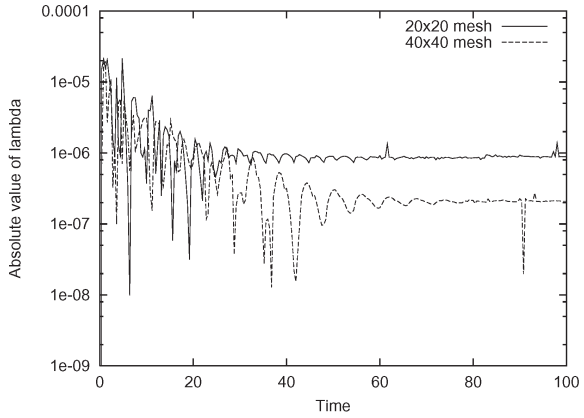


Figure 10: Time history of Lagrange multiplier $|\lambda_h|$(Case A1 and A3).

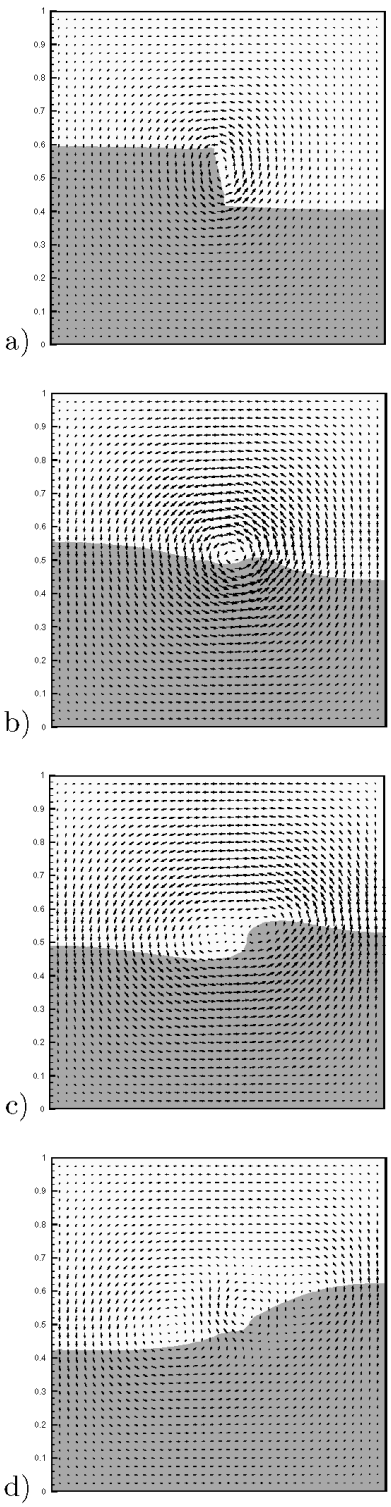


Figure 11: Velocity vector and interface at (a) $t = 0.1$, (b) $t = 0.3$, (c) $t = 0.5$, (d) $t = 0.7$, (Case B1).

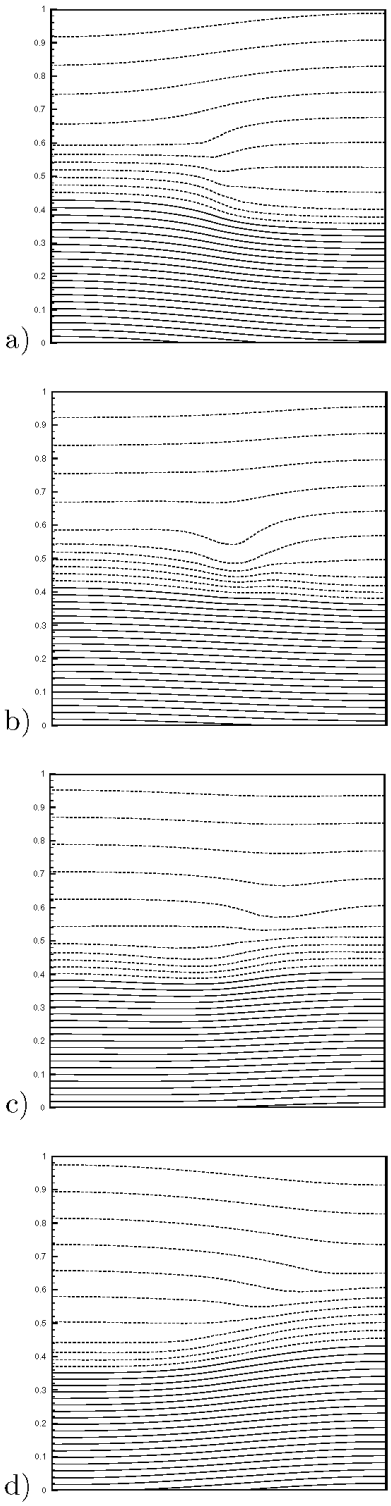


Figure 12: Pressure contours at (a) $t = 0.1$, (b) $t = 0.3$, (c) $t = 0.5$, (d) $t = 0.7$, (Case B1).

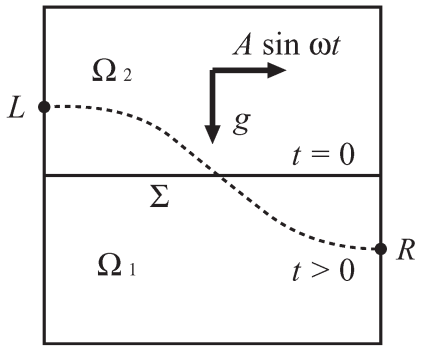


Figure 13: Sloshing tank problem

Reynolds number flows. Here we assume that $\mu_1 = \mu_2$ and $\rho_1 > \rho_2$. Fluid properties and other parameters are summarized in table 5.2 and 5.2, respectively. We also impose the free-slip condition on the boundary of the domain $\Omega$. The computations were performed on the same triangulations in Sect. 5.1.

Table 3: Fluid properties

| set | $\rho_1$ | $\mu_1$ | $\rho_2$ | $\mu_2$ | $a$ | $\beta$ |
|---|---|---|---|---|---|---|
| C | 1.0 | 0.01 | 0.91 | 0.01 | 0.05 | 0.0625 |
| D | 1.0 | 0.001 | 0.91 | 0.001 | 0.25 | 0.125 |

Table 4: Cases computed for sloshing problem

| case | Mesh (Union-Jack) | Total time $T$ | Time steps $[T/\Delta t]$ | Flux functional | Property set |
|---|---|---|---|---|---|
| C1 | $20 \times 20$ | 200 | 5000 | Yes | C |
| C2 | $20 \times 20$ | 200 | 5000 | No | C |
| C3 | $40 \times 40$ | 200 | 10000 | Yes | C |
| C4 | $40 \times 40$ | 200 | 10000 | No | C |
| D1 | $20 \times 20$ | 100 | 5000 | Yes | D |
| D2 | $20 \times 20$ | 100 | 5000 | No | D |
| D3 | $40 \times 40$ | 100 | 10000 | Yes | D |
| D4 | $40 \times 40$ | 100 | 10000 | No | D |

Figure 14 shows the time histories of the elevation of the interface at the left and right sides of container for both our proposed method and the method without flux functional in a low Reynolds number flow (the set C). As well as the results in previous problem, we observe that our method gives almost same phenomena as the method without flux functional at least in the behavior at the left and right sides, however, we also find that the method without the flux functional gives non-zero flux during the computation time as shown in Figures

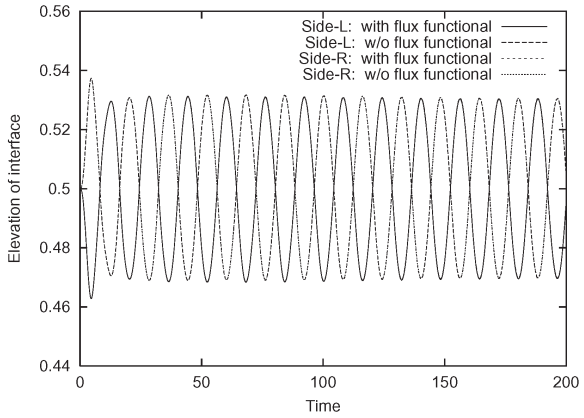


Figure 14: Time history of elevation of the interface at the sides L and R(Case C1 and C2).

15 and 16. Figure 17 shows the time histories of the Lagrange multiplier for the case C1 and C2. From this results, we also observe that the Lagrangian multiplier converges to 0 very slowly.

On the other hand, the results in high Reynolds number case D are very interesting. We can observe some difference between two methods for the time histories of elevation of the interface as shown in Figures 18 and 19. Furthermore, we can observe considerably disrupted flux in Figures 20 and 21. In fact these phenomena may be proved by the large deformation of the interface as shown in Figure 23. This suggests that in high Reynolds number flows the usual method without the flux functional may not preserve the mass of the fluid, but our proposed method may withstand the large deformation of the interface with good mass preserving.

# 6 Conclusion

We have introduced the flux-free finite element method using Lagrange multiplier for immiscible two-fluid flows. The study was focused on the numerical scheme of this method and its numerical performance. In such a context, three main points have been addressed: (1) our proposed method shows the good mass preserving by the almost zero numerical flux and (2) the cause of the gain or loss of the fluid mass is the producing the numerical flux on the interface during the numerical computations, and (3) the algorithm is easy to code the initial Eulerlian mesh remains the same throughout computation.

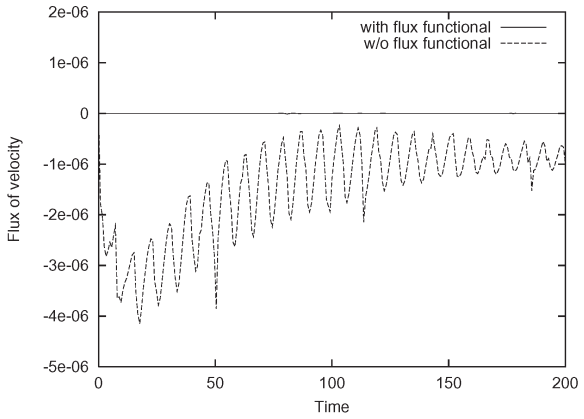


Figure 15: Time history of flux of velocity through the interface(Case C1 and C2).

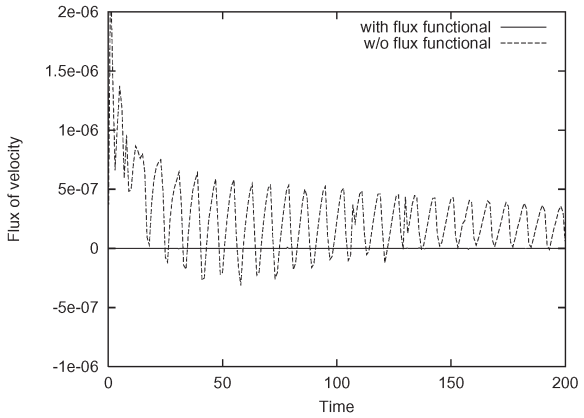


Figure 16: Time history of flux of velocity through the interface(Case C3 and C4).

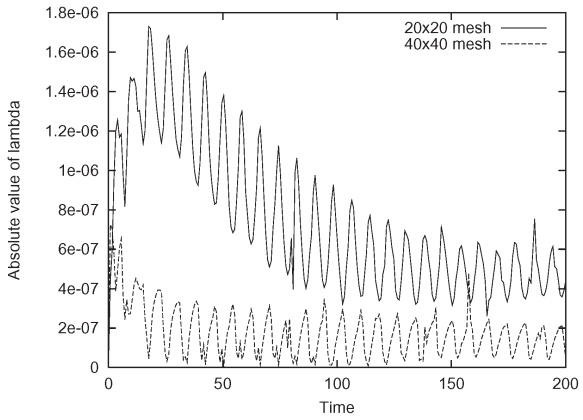


Figure 17: Time history of Lagrange multiplier $|\lambda_h|$(Case C1 and C2).

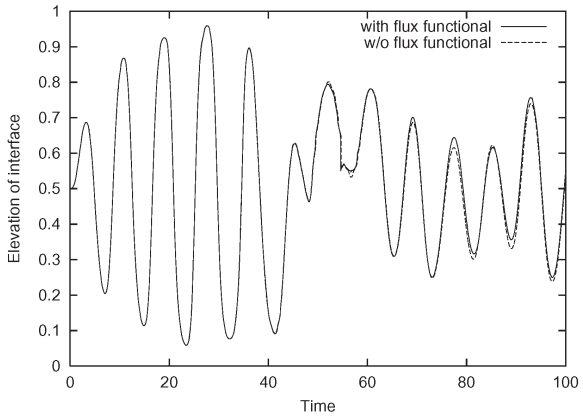


Figure 18: Time history of elevation of the interface at the side R.(Case D1 and D2).

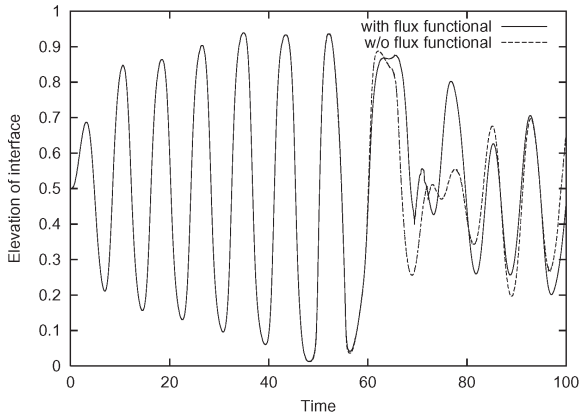


Figure 19: Time history of elevation of the interface at the side R.(Case D3 and D4).

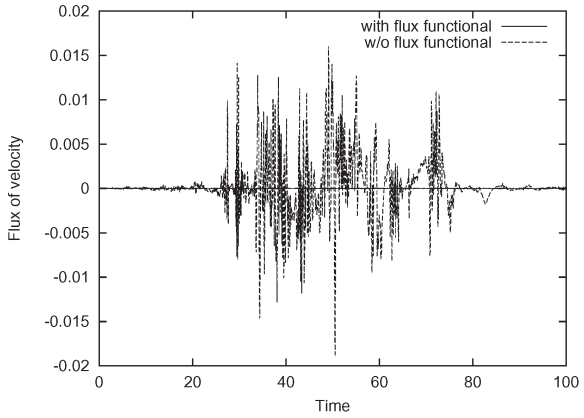


Figure 20: Time history of flux of velocity through the interface(Case D1 and D2).

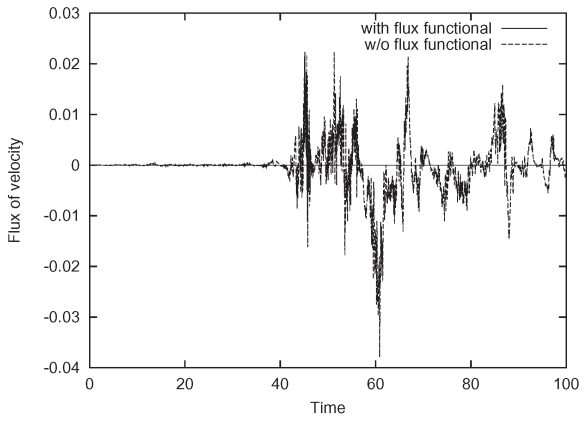


Figure 21: Time history of flux of velocity through the interface.(Case D3 and D4).

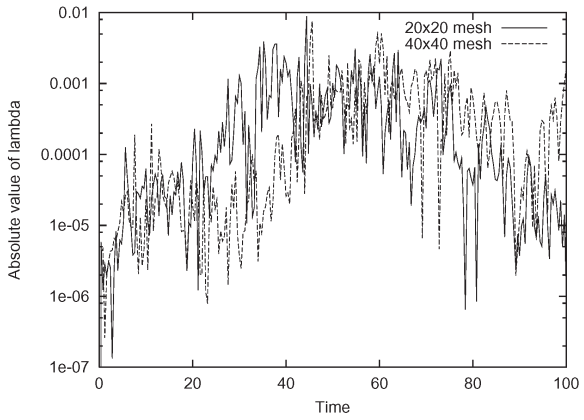


Figure 22: Time history of Lagrange multiplier $|\lambda_h|$(Case D1 and D3).

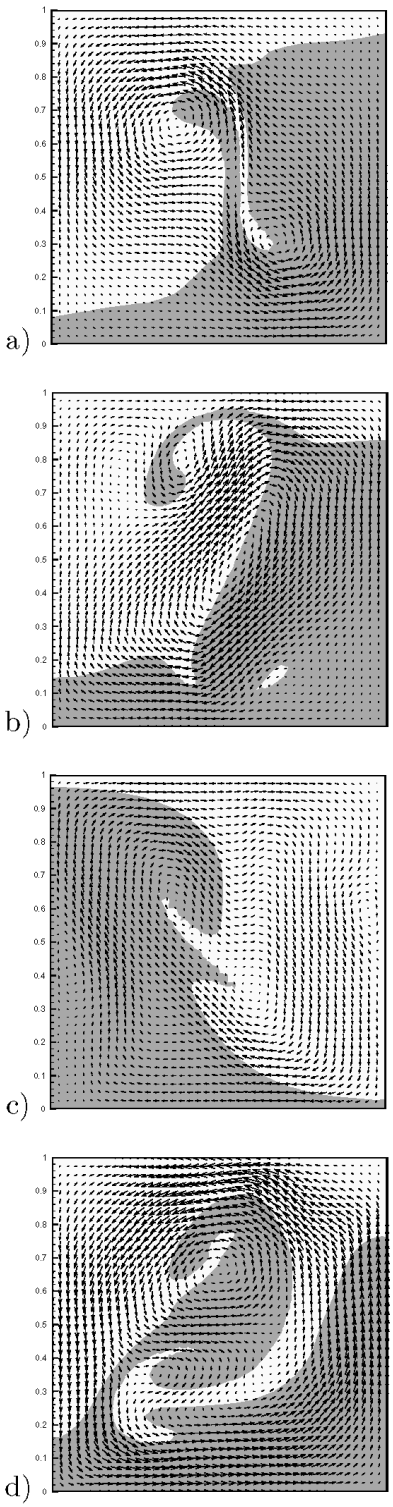


Figure 23: Velocity vector and interface at (a) $t = 43.1$, (b) $t = 44.5$, (c) $t = 47.3$, (d) $t = 50.8$(Case D3).

## Acknowledgments

The authors thank Dr. N. Saito of University of Toyama for his useful discussion. This work was partially supported by the Grant-in-Aid for Scientific Research((C)(2) No. 15540113) of Japan Society for the Promotion of Science.

## References

[1] Baiocchi C., Brezzei F., Franca L.P., Virtual bubbles and Galerkin-least-squares type methods (Ga.L.S.), *Computer Methods in Applied Mechanics and Engineering*, **105**(1993), pp.125–141.

[2] Brooks A.N., Hughes T.J.R., Streamline upwind/Petrov-Galerkin formulation for convection dominated flows with particular emphasis on the incompressible Navier-Stokes equations, *Computer Methods in Applied Mechanics and Engneering*, **32**(1982), pp.199-259.

[3] Cruchaga M., Celentano D., Tezduyar T., A moving Lagrangian interface technique for flow computations over fixed meshes, *Computer Methods in Applied Mechanics and Engneering*, **191**(2001), pp.525–543.

[4] Formaggia F., Gerbeau J.-F., Nobile F., Quarteroni A., Numerical treatment of defective boundary conditions for the Navier-Stokes equations, *SIAM Journal of Numerical Analysis*, **40**(2002), pp.376–401.

[5] Franca L.P., Frey S.L., Stabilized finite element methods: II. The incompressible Navier-Stokes equations, *Computer Methods in Applied Mechanics and Engneering*, **99**(1992), pp.209–233.

[6] Hirt C,W., Nichols B.D., Volume of fluid (VOF) method for the dynamics of free boundaries. *Journal of Computational Physics*, **39**(1981), pp.201–225.

[7] Jeong J.H., Yang D.Y., Finite element analysis of transient fluid flow with free surface flow using VOF (Volume-of-Fluid) method and adaptive gird, *International Journal for Numerical Methods in Fluids*, **26**(1998), pp.1127-1154.

[8] Kim M.S., Lee W.I., A new VOF-based numerical scheme for the simulation of fluid fow with free surface. Part I: New free surface-tracking algorithm and its verification, *International Journal for Numerical Methods in Fluids*, **42**(2003), pp.765–790.

[9] Ohmori K., Convergence of the interface in the finite element approximation for two-fluid flows, R. Salvi. ed., *the Navier-Stokes equations: theory and numerical methods*, Lecture Notes in Pure and Applied Mathematics, Marcel Dekker, **223**(2002), pp.279–293.

[10] Ohmori K., Fujima S., Fujita Y., Convergence analysis of interface for interfacial transport phenomena. *Mathematics of Toyama University*, **26**(2003), pp.279–293.

[11] Ohmori K., Saito N., Flux-free finite element method with Lagarange multipliers for two-fluid flows, *Journal of Scientific Computing*, **32**(2007), pp.147–173.

[12] Ohmori K., Saito N., Okumura H., Mass conserevative finite element method for free interface flows. *Proceedings of ECCOMAS* 2004, Jyväskylä, Finland.

[13] Okumura H., Kawahara M., A new stable bubble element for incompressible fluid flow based on a mixed Petrov-Galerkin finite element formulation, *International Journal of Computational Fluid Dynamics*, **17**(2003), pp.275–282.

[14] Pierre R., Optimal selection of the bubble function in the stabilization of the $P^1$-$P^1$ element for the Stokes problem. *SIAM Journal on Numerical Analysis*, **32**(1995), pp.1210–1224.

[15] Sussman M., Smereka P., Osher S., A level set approach for computing solutions to incompressible two-phase flow, *Journal of Computational Physics*, **79**(1988), pp.12–49.

[16] Yamada T., A bubble element for the compressible Euler equations. *International Journal of Computational Fluid Dynamics*, **9**(1998), pp.273–283.

[17] Zhang S.-L., GPBi-CG: Generalized product-type methods based on Bi-CG for solving nonsymmetric linear systems, *SIAM Journal on Scientific Computing*, **18**(1997), pp.537–551.

Katsushi OHMORI
Department of Mathematics
Faculty of Human Development
University of Toyama
3190 Gofuku, Toyama
930-8555 Japan
ohmori@edu.u-toyama.ac.jp

Hiroshi OKUMURA
Information Technology Center
University of Toyama
3190 Gofuku, Toyama
930-8555 Japan
okumura@itc.u-toyama.ac.jp

（2007年 5 月17日受付）
（2007年 7 月 4 日受理）